


Control of electron and ion density profiles via virtual ground position control in an inductively coupled plasma

Cite as: Phys. Plasmas **27**, 073505 (2020); <https://doi.org/10.1063/5.0010018>

Submitted: 06 April 2020 . Accepted: 10 June 2020 . Published Online: 07 July 2020

Tae-Woo Kim, Ju-ho Kim, Moo-Young Lee, and  Chin-Wook Chung

COLLECTIONS

 This paper was selected as Featured



View Online



Export Citation



CrossMark

ARTICLES YOU MAY BE INTERESTED IN

[Global model for pulsed inductively coupled plasma sources: Effect of edge-to-center density ratio and electron heating](#)

Phys. Plasmas **27**, 073507 (2020); <https://doi.org/10.1063/5.0006505>

[Review of pulsed power-driven high energy density physics research on Z at Sandia](#)

Phys. Plasmas **27**, 070501 (2020); <https://doi.org/10.1063/5.0007476>

[Review of inductively coupled plasmas: Nano-applications and bistable hysteresis physics](#)

Applied Physics Reviews **5**, 011108 (2018); <https://doi.org/10.1063/1.5012001>



Physics of Plasmas
Features in Plasma Physics Webinars

Register Today!

Control of electron and ion density profiles via virtual ground position control in an inductively coupled plasma

Cite as: Phys. Plasmas **27**, 073505 (2020); doi: [10.1063/5.0010018](https://doi.org/10.1063/5.0010018)

Submitted: 6 April 2020 · Accepted: 10 June 2020 ·

Published Online: 7 July 2020



View Online



Export Citation



CrossMark

Tae-Woo Kim,^{1,a)} Ju-ho Kim,¹ Moo-Young Lee,² and Chin-Wook Chung^{1,b)} 

AFFILIATIONS

¹Department of Electrical Engineering, Hanyang University, Seoul 133-791, South Korea

²Department of Nanoscale Semiconductor Engineering, Hanyang University, Seoul 133-791, South Korea

^{a)}E-mail: worldcorn2002@nate.com

^{b)}Author to whom correspondence should be addressed: joykang@hanyang.ac.kr

ABSTRACT

The effects of capacitive coupling on electron and ion density profiles are studied in an argon inductively coupled plasma. Electron energy probability functions and two-dimensional ion density profiles were measured by changing the termination capacitance from 200 to 1000 pF. Experimental results show that a termination capacitor creates a virtual ground on a coil, and the virtual ground suppresses the local capacitive coupling. At 2 mTorr (non-local electron kinetics), there is little change in the azimuthal electron density distribution for different termination capacitances. However, at 50 mTorr (local electron kinetics), the virtual ground causes each mode (E-mode and H-mode) to have the maximum and minimum points in the azimuthal electron density distribution. As the termination capacitance increases, the virtual ground moves along the coil and the maximum and minimum points of the electron density also move with the virtual ground. These effects are explained by electron dynamics and the power transfer mechanism in each mode (E-mode and H-mode).

Published under license by AIP Publishing. <https://doi.org/10.1063/5.0010018>

I. INTRODUCTION

In recent decades, significant advances have been made in semiconductor and display manufacturing using various characteristics of plasmas.^{1–3} As feature size decreases in microelectronics, the precise control of plasma processes has become more important to achieve successful plasma etching.^{4,5} Inductively coupled plasma (ICP) sources are primarily used as dry etching sources^{6–9} because of their advantages such as high electron density at low pressure and independent ion energy control by coupling substrate bias.^{10,11}

ICPs have many distinct characteristics over the other RF plasma sources, but the most distinguishable characteristic is their E to H mode transition.^{12–15} E-mode occurs in the low RF power regime, in which the capacitive field between an antenna coil and the ground accelerates electrons and sustains the discharge. The capacitive coupling is necessary to transfer the RF power from the antenna to the plasma at E-mode. As RF power increases, the sheath length becomes shorter due to the increase in electron density. Because of the short sheath length, the impedance of the sheath decreases, the voltage distributed to the quartz window increases, and the voltage across the sheath decreases. As a result, the capacitive field in the sheath is

suppressed. At the same time, power absorption by the electromagnetic field is enhanced, causing a mode transition from the E-mode (capacitive coupling discharge) to the H-mode (inductive coupling discharge).⁹ This heating mode transition is accompanied by hysteresis, and the hysteresis loop can be changed by the discharge pressure, initial matching situation, electron density distribution, and multistep ionization.^{15–20} In H-mode, in contrast to E-mode, the RF power is transferred to the plasma by the electric field induced by a time-varying magnetic field. In this regime, the capacitive coupling from the coil to the plasma causes additional ion energy loss and reduces the electron density.

Capacitive coupling accelerates ions toward the substrate and dielectric window. These accelerated ions cause impurity problems by sputtering metal wall and dielectric window. To overcome these problems, several studies have been carried out to reduce capacitive coupling between an antenna coil and the plasma, such as a Faraday shield,^{21–23} a parallel structure antenna,²⁴ a DC superposing on an antenna,²⁵ and a termination capacitor.^{26,27} Additional attempts to solve this problem include Yoshida *et al.*,²⁸ modifying the dielectric window shape; Kim *et al.*,²⁹ reducing the voltage of the coil using an

external magnetic field; and Zheng *et al.*,³⁰ placing the coil ground on a dielectric window. Of the various possible solutions, the termination capacitors are among the most widely used in plasma processes because of the simple structure and effective suppression of the capacitive coupling. The termination capacitor (capacitance C) creates a virtual ground on the coil (inductance L), and at the characteristic capacitance when the termination reactance $[1/(\omega C)]$ coincides with a half of the coil reactance $(\omega L/2)$, the virtual ground is located in the middle of the antenna, creating a voltage standing wave and significantly canceling the capacitive coupling between the coil and the plasma.^{26,27} This characteristic condition is called the balanced condition. Optical emission measurements for the presence and absence of a capacitor in the balanced condition were studied by Edamura and Benck.³¹ Many studies on termination capacitors have been conducted, but few have investigated the effect of termination capacitance on the spatial plasma distribution.

The spatial distribution of the plasma is very important because it is directly related to the process results and a uniform plasma is required to improve process yield.^{32–34} The virtual ground has zero potential with respect to ground, and the vicinity of the virtual ground has the weakest capacitive coupling within the coil and a very weak electrostatic field.^{27,35,36} If the termination capacitance changes, the virtual ground moves along the antenna. This movement of the virtual ground changes the voltage distribution along the coil and causes a spatial change of the local capacitive coupling. The change of the local capacitive coupling can change the electron density profile. Therefore, a study on the spatial variation of plasma parameters with the termination capacitance is required.

In this paper, we investigate the changes of electron and ion density profiles with changing termination capacitance in an argon plasma. The dependence of electron density on termination capacitance varies with mode and pressure. The change in the electron and ion density profiles with the termination capacitance is clearly seen at high pressure.

II. EXPERIMENTAL SETUP

Experiments were performed in a reactor as shown in Fig. 1. The reactor has a cylindrical shape with an inner diameter of 40 cm and a

height of 15 cm. RF power of 13.56 MHz was applied to a single-turn coil through an impedance matching network. RF power of 20 W was applied for E-mode discharge, whereas 300 W of RF power was applied for H-mode discharge. The matching network had a standard type circuit, which consists of two vacuum variable capacitors. The reflection of RF power was maintained under 1% of the applied power. The termination capacitor was connected in series with the antenna coil, and its capacitance was varied from 200 to 1000 pF. The base pressure was kept lower than 8×10^{-6} Torr by a rotary vane pump and turbo molecular pump. Argon gas was used, and the pressures were measured using a capacitive manometer gauge (CMG). The gas flow rate was maintained at 15 SCCM. The top wall was covered with quartz of 2 cm thickness. A single-turn coil with a diameter of 20 cm was placed on the quartz. Water was flowed in the coil to prevent temperature effect on the coil resistance. To measure the terminal voltages V_1 and V_2 , two high-voltage probes were installed at terminal 1 and terminal 2, respectively. The output of the high-voltage probes was connected to a digital oscilloscope. V_1 is the voltage of the start position of the coil, and V_2 is the voltage of the end of the coil. A RF-compensated Langmuir probe made of tungsten wire (10 mm in length and 0.1 mm in diameter) was placed 8 cm below the quartz. The RF choke filter resonates at 13.56 MHz and its second harmonic of 27.12 MHz to compensate RF fluctuation.³⁷ To obtain electron density and radial density distributions, the electron energy probability function (EEPF) was measured. The second derivative of probe current I_p is proportional to EEPF $f_e(\varepsilon)$ as follows:

$$f_e(\varepsilon) = \frac{2m_e}{e^2 A} \left(\frac{2e\varepsilon}{m_e} \right)^{\frac{1}{2}} \frac{d^2 I_p(V)}{dV^2}, \quad (1)$$

where ε , m_e , e , A , and I_p are the electron energy, the electron mass, the electron charge, the probe area, and the probe current, respectively. The EEPF is related to the electron energy distribution function (EEDF) $f_e(\varepsilon) = \varepsilon^{1/2} g_e(\varepsilon)$ as follows:

$$g_e(\varepsilon) = \frac{2m_e}{e^2 A} \left(\frac{2e\varepsilon}{m_e} \right)^{\frac{1}{2}} \frac{d^2 I_p(V)}{dV^2}. \quad (2)$$

Electron density n_e is obtained from the integral of the EEDF³ as

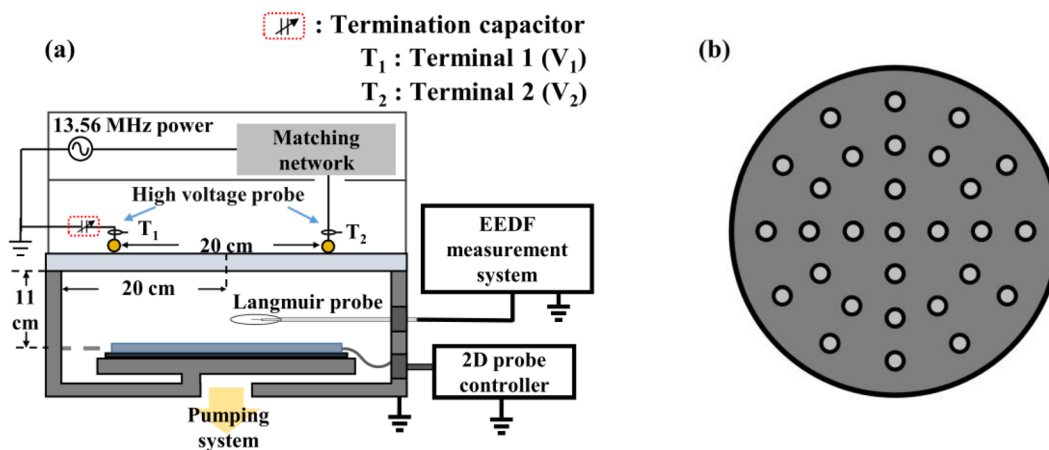


FIG. 1. (a) Experimental setup and (b) two-D probe arrangement.

$$n_e = \int_0^\infty g_e(\varepsilon) d\varepsilon. \tag{3}$$

To obtain two-dimensional ion density profiles, a wafer-type probe³⁸ with a diameter of 30 cm was installed 11 cm below the quartz, and the ion density profiles were measured based on the floating harmonic method.³⁹ When a small sinusoidal voltage ($v_0 \cos \omega t$) is applied to the probe tip, the measured current has harmonics due to the non-linearity of the sheath. Comparing the ratio of the amplitudes of the first and second harmonics, the electron temperature can be obtained. The electron temperature, T_e , and the ion density, n_i , are given as follows:⁴⁰

$$T_e \approx \frac{v_0 I_\omega}{4 I_{2\omega}} \quad (v_0 < T_e), \tag{4}$$

$$n_i = \frac{I_\omega T_e}{0.61 e u_B A v_0}, \tag{5}$$

where v_0 , I_ω , $I_{2\omega}$, u_B , and A are the amplitude of the probe bias voltage, the current of a fundamental frequency, the current of the second harmonic, the Bohm velocity, and the probe area, respectively. A quasi-stationary sheath and constant ion flux are assumed.⁴¹ The wafer-type probe, which consists of 29 probe tips, has a radius of 15 cm, and each probe tip has a diameter of 15 mm.

III. EXPERIMENTAL RESULT

Figures 2(a) and 2(b) show the radial electron density profiles at the pressures of 2 mTorr and 50 mTorr. A fixed RF power of 20 W for E-mode and 300 W for H-mode was applied. At 2 mTorr, the electron density is maximized at the center of the plasma. As pressure increases to 50 mTorr, the electron density is maximized near the coil. When the termination capacitance increases from 200 pF to 400 pF, the maximum density of the radial electron density decreases in E-mode but increases in H-mode. As the termination capacitance increases from 400 pF to 1000 pF, the maximum radial electron density increases in E-mode and decreases in H-mode. Remarkably, the electron density variation with the termination capacitance is larger at higher pressures and in E-mode.

The measured voltages V_1 and V_2 as a function of termination capacitance are shown in Fig. 3. As the termination capacitance increases from 200 pF to 1000 pF, V_1 monotonically increases and V_2 monotonically decreases. At $C = 200$ pF, V_1 is about 30 V. In this condition, the reactance of the coil is almost canceled by the reactance of the capacitor, and a virtual ground is created near terminal 1. At $C = 400$ pF, V_1 and V_2 are the same, and the virtual ground is created at the middle of the coil. At $C = 1000$ pF, when V_2 is between 200 V and 300 V, the reactance of the capacitor is small, so it can hardly

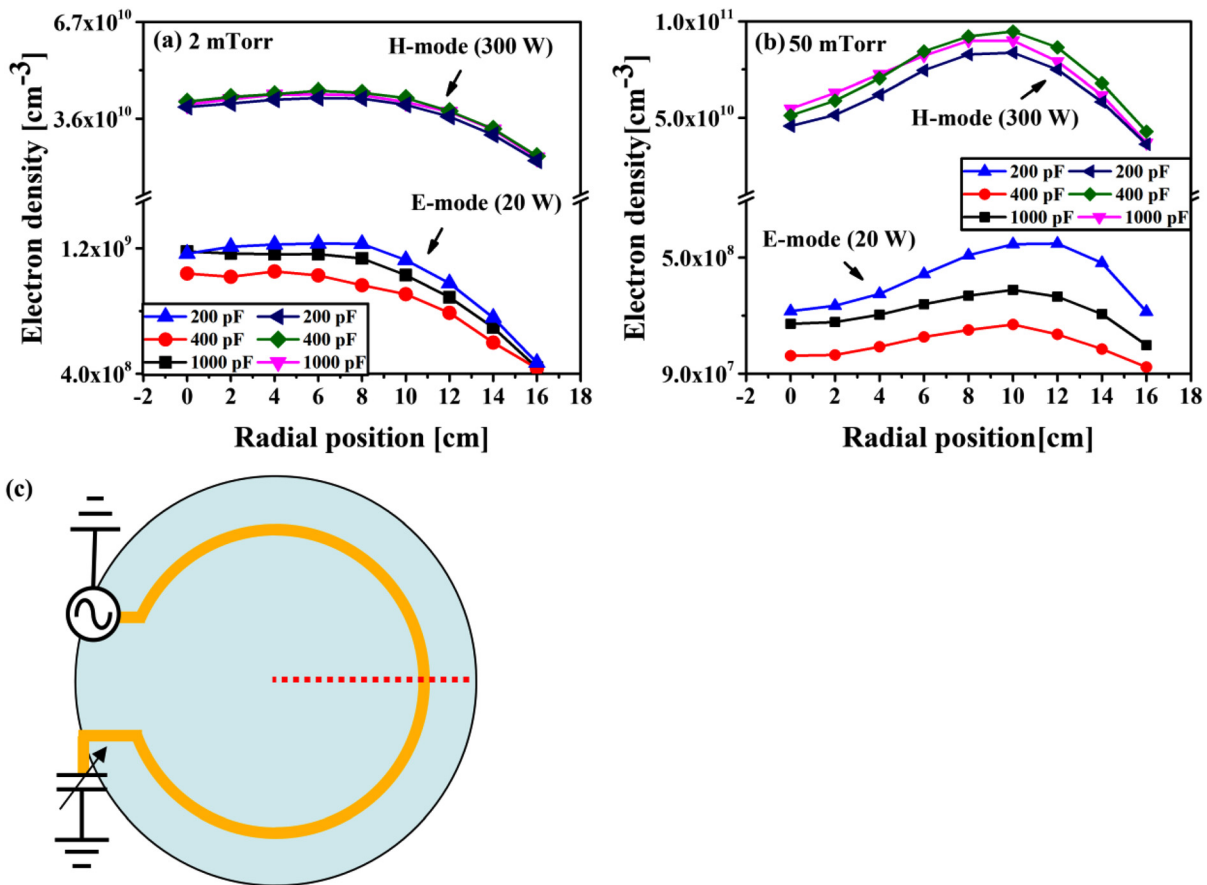


FIG. 2. Radial electron density profiles for various termination capacitances at (a) 2 and (b) 50 mTorr. (c) The radial measurement position of the electron density profiles.

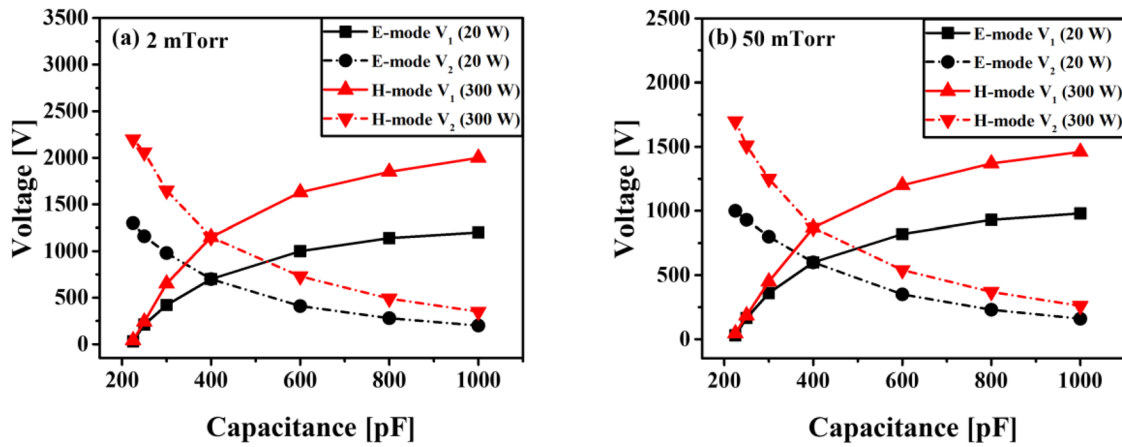


FIG. 3. Measured terminal voltages V_1 and V_2 as a function of termination capacitance at pressures of (a) 2 and (b) 50 mTorr.

cancel the reactance of the coil. As a result, the virtual ground is created in front of the termination capacitor. These data demonstrate that the position of the virtual ground changes with the capacitance. The positions of the virtual ground for different termination capacitances are shown in Figs. 4(a) and 4(b).

If the material and structure of the coil are constant, the resistance and reactance per unit length of the coil are constant, and the voltage distribution along the coil is linear. In our experiment, since the coil is made of copper of constant thickness, the voltage distribution along the coil is linear. Therefore, to investigate the virtual ground position, we obtained the linear distribution of voltage along the coil based on the measured voltages of V_1 and V_2 . Figure 4(a) shows the linear voltage distribution along the coil for different capacitances at 50 mTorr in H-mode. Here, we define the length of the coil from terminal 1 to terminal 2 as d and the distance along the coil from terminal 1 as r . In Fig. 4(a), red circles are the points where the potential is 0 V in the voltage distribution, where a virtual ground is created. As termination capacitance increases from 200 pF to 1000 pF, the virtual ground moves from near terminal 1 to near the terminal 2. If the

termination capacitance is infinitely large, the voltage of terminal 2 will be 0 (like a grounded coil). However, at 1000 pF, since the termination capacitance is not large enough to ignore the impedance of the termination capacitor, the virtual ground is created at about 0.8d. The virtual ground moves along the coil clockwise with increasing termination capacitance as shown in Fig. 4(b). Near the virtual ground of the antenna, the voltage is close to 0 and the capacitive coupling is suppressed.^{26,27} Therefore, the electron density profiles can be changed with termination capacitance.

As shown in Fig. 2, the pressures of 2 mTorr and 50 mTorr have different radial electron density profiles, and there is a difference in change of the radial electron density profile with the termination capacitance. At 2 mTorr, there is little change in the electron density profile. However, at 50 mTorr, the electron density near the coil changes significantly with the capacitance. These differences can be explained by the dependence of electron kinetics on the pressure.

At low pressure, where the electron energy relaxation length λ_e is longer than the discharge length l , the electrons are heated near the coil and can travel the entire volume of the plasma before they lose

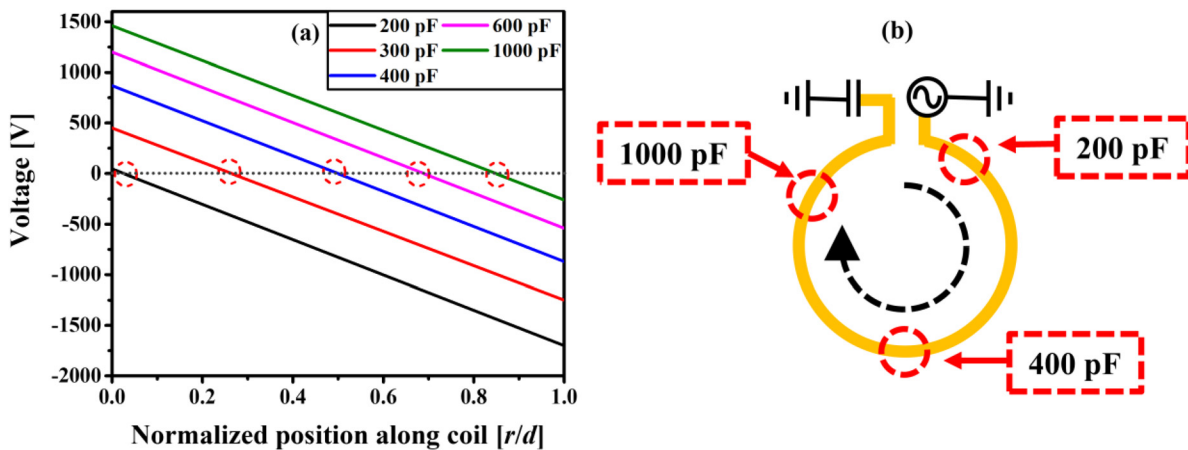


FIG. 4. (a) Calculated voltage distributions along the coil for different capacitances at 50 mTorr in H-mode. (b) The virtual ground position on the coil.

their energy. The electron kinetics which has difference between maximum electron heating region and maximum ionization region has been well studied and is referred to as “non-local electron kinetics.”^{42–45} In this regime, as shown in Fig. 2(a), the electron density is maximum at the center of the plasma and decreases gradually toward the boundaries. At low pressure, the plasma potential is maximal at the center of the plasma due to ambipolar diffusion.^{3,46} Electrons experience the ambipolar potential as a potential wall to overcome. Electrons have kinetic energy and potential energy, and if there are no collisions, the sum of these two energies is conserved. Therefore, electrons have maximal kinetic energy at the center of plasma where the plasma potential is maximized. For this reason, in the low pressure and non-local electron kinetics regime, maximum ionization occurs at the center of plasma. At high pressure, the electron energy relaxation length decreases due to frequent electron–neutral collisions. In this regime, the electrons are heated near the antenna coil and lose their energy in the same region before reaching the center of the plasma. Therefore, the plasma density is maximum near the antenna coil in this local kinetics. To verify the electron kinetics, λ_e was compared to the discharge length, l . The electron energy relaxation length in inelastic range can be written as³

$$\lambda_e \approx \left(\frac{\lambda_m \lambda_{inel}}{3} \right)^{\frac{1}{2}}, \quad (6)$$

where λ_m is the total mean free path for momentum transfer and λ_{inel} is the mean free path accounting for all collisional energy loss process. λ_{inel} is as follows:

$$\lambda_{inel}^{-1} = n_g \left[\left(\frac{2m}{M} \right) \sigma_{el} + \sigma_{ex} + \sigma_{iz} + \dots \right], \quad (7)$$

where n_g , M , σ_{el} , σ_{ex} , and σ_{iz} are the neutral gas density, the neutral gas mass, the elastic collision cross section, the excitation collision cross section, and the ionization collision cross section, respectively. The collision cross section data for argon gas are obtained from the Biagi database.⁴⁷ In our experiments, at 2 mTorr, the electron energy relaxation length is 60 cm for ionization (15.76 eV). Since λ_e exceeds the discharge length l , the electrons are governed by the non-local

kinetics. Therefore, at 2 mTorr, the radial electron density profiles are determined by ambipolar diffusion and do not change with the termination capacitance, as shown in Fig. 2(a). However, at 50 mTorr, the λ_e is 2.4 cm for the ionization (15.76 eV), which is shorter than discharge length l . In this regime, the electrons are governed by local electron kinetics, and the electron density profiles are determined by local heating and local ionization. Therefore, at 50 mTorr, the local capacitive coupling, which changes with the position of the virtual ground, changes the local heating and local energy loss, resulting in a significant change in the radial electron density profiles. To investigate the change of the local electron density with the virtual ground position, the EEPFs are measured at a fixed position below the coil midpoint with increasing termination capacitance from 200 pF to 1000 pF.

As shown in Fig. 5(c), a Langmuir probe is placed under the midpoint of the coil. Figures 5(a) and 5(b) indicate that at $C = 400$ pF, for which the virtual ground is closest to the measurement point, the electron densities are maximized in H-mode and minimized in E-mode. The variation of the electron density is small in H-mode, while it is remarkably large in E-mode. The observed electron density variations with increasing the termination capacitance from 200 pF to 400 pF at 2 mTorr are 7% in H-mode and 19% in E-mode, and at 50 mTorr, the electron density variations are 4% in H-mode and 50% in E-mode. The suppression of local capacitive coupling near the coil is clearly seen in the EEPFs.

Figure 6 shows the EEPFs in a total energy scale (sum of kinetic and potential energies) at 2 mTorr. The EEPFs are measured at the same measurement point as shown in Fig. 5(c). In E-mode [Fig. 6(a)], the EEPFs exhibit a bi-Maxwellian distribution,^{48,49} which has two temperatures. In H-mode [Fig. 6(b)], the EEPFs exhibit a Maxwellian-like distribution.³ This is a typical characteristic of low-pressure argon discharge. At low electron density and low pressure for argon discharge, EEPFs are a bi-Maxwellian distribution because of the Ramsauer minimum^{48,50} and ambipolar potential well. Low energy electrons, which are generated by ionization, cannot overcome the ambipolar potential well, and the Ramsauer minimum prevents Ohmic heating of the low energy electrons in the argon discharge. Therefore, the low energy electrons are confined within the plasma bulk, and only high energy electrons overcome the ambipolar potential

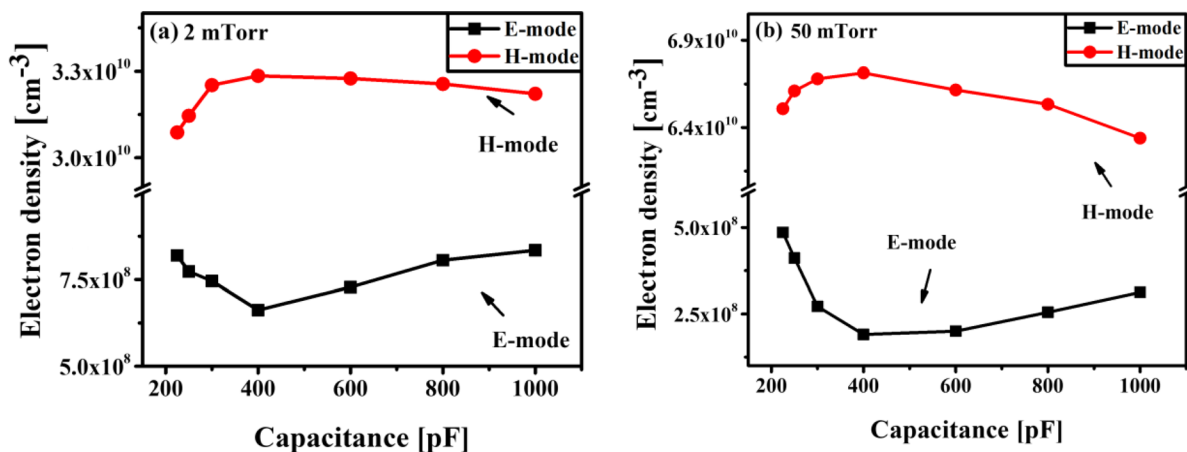


FIG. 5. Electron densities under the midpoint of the coil as a function of termination capacitance at (a) 2 and (b) 50 mTorr and (c) the position of these measurements.

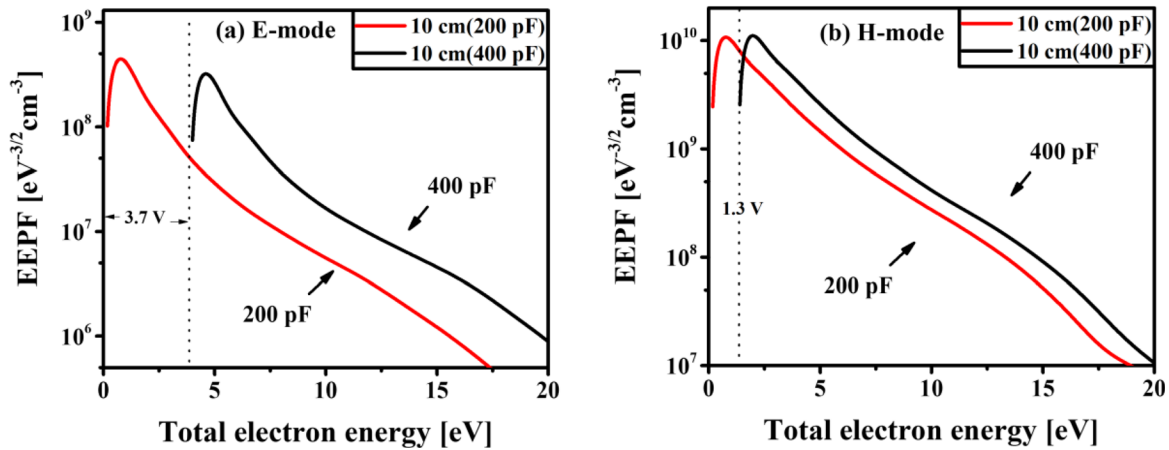


FIG. 6. (a) E-mode EPPFs at 2 mTorr (200 pF, 400 pF). (b) H-mode EPPFs at 2 mTorr (200 pF, 400 pF).

and reach the heating region. In H-mode, the EPPF becomes Maxwellian-like due to frequent electron–electron collisions.^{3,48} As shown in Fig. 6, the EPPFs in a total energy scale have different starting points for 200 pF and 400 pF, which indicates a difference in potential energy. This difference in potential energy indicates a difference in plasma potential and shows suppression of capacitive coupling. In E-mode [Fig. 6(a)], the plasma potential difference between 200 pF and 400 pF is 3.7 V, and the electron density is decreased. In H-mode [Fig. 6(b)], the plasma potential is reduced by 1.3 V at 400 pF compared to 200 pF, and the electron density is increased.

Figure 7 shows the EPPFs in a total electron energy scale at 50 mTorr. In E-mode, the EPPFs are Druyvesteyn-like distribution.⁵¹ This distribution is typical for an argon discharge in low-frequency fields ($\nu_{en}^2 \gg \omega^2$) with few electron–electron collisions.^{48,52} In this condition, low-energy electrons have high temperature and high-energy electrons have low temperature. Low-energy electrons accelerate with few electron–neutral collisions due to the Ramsauer minimum; therefore, electron temperature of low-energy electron group is increased. On the other hand, since inelastic electron–neutral

collisions occur frequently, high-energy electrons are depleted and the high-energy group temperature is decreased. In H-mode, EPPFs become Maxwellian distribution due to increased electron–electron collisions. In E-mode [Fig. 7(a)], the plasma potential difference is 7 V, and the electron density is decreased significantly. In H-mode [Fig. 7(b)], as the termination capacitance increases, the plasma potential reduced by 0.9 V and the electron density is increased slightly. Figures 6 and 7 show that the suppression of the capacitive coupling with the termination capacitance is small in H-mode but very large in E-mode. The difference in the capacitive coupling suppression effect between E-mode and H-mode can be understood by the power transfer mechanism in each mode.

In H-mode, the sheath length is short due to the high electron density. Since the impedance of the sheath is small, only a small fraction of V_{RF} appears across the sheath.³ In this regime, most of the RF power is transferred through inductive coupling, and very small amounts of RF power are transferred through the capacitive coupling.¹⁴ As a result, the suppression of capacitive coupling has little effect on the power transfer, and the electron density variation and the

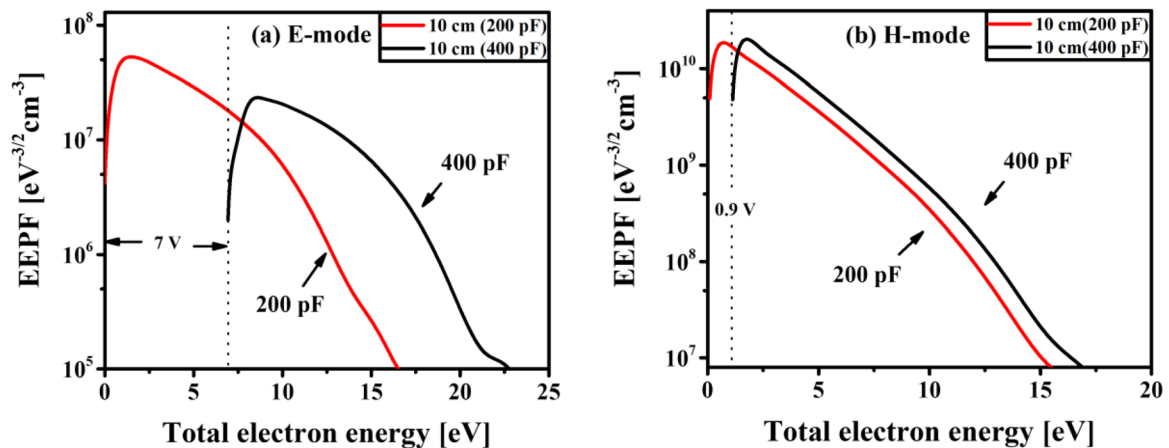


FIG. 7. (a) E-mode EPPFs at 50 mTorr (200 pF, 400 pF). (b) H-mode EPPFs at 50 mTorr (200 pF, 400 pF).

suppression of the capacitive coupling are very minimal in H-mode. However, In E-mode, since the electron density is low, the sheath length is long, and high voltage is applied across the sheath. This high voltage enhances the E-field within the sheath, and the E-field delivers RF power to the plasma. Since almost all RF power is transferred through capacitive coupling, electron density variation and suppression of the capacitive coupling are very significant.

Our experimental results show that the virtual ground moves with the termination capacitance and changes the local capacitive coupling. At high pressure (local electron kinetics regime), the change of the local capacitive coupling changes the electron density profiles significantly. These results imply that the azimuthal electron density distribution will have a maximum in H-mode and a minimum in E-mode. If the termination capacitance increases, the virtual ground will rotate clockwise along the coil, and the maximum and minimum points of electron density in H-mode and E-mode are expected to move along with the virtual ground. To verify the effect of virtual ground on azimuthal density variation, two-dimensional ion densities were measured under the same experimental conditions.

Two-dimensional ion density profiles at 50 mTorr in E-mode are shown in Fig. 8. Yellow circles indicate the minima of the azimuthal ion density distributions along the coil. As shown in Fig. 2(b), the radial profiles are concave. The positions of the minima in the azimuthal ion density distributions in E-mode agree well with those of the virtual ground, as shown in Figs. 4(a) and 4(b). The minimum point of ion density moves clockwise with an increase in the termination capacitance from 200 pF to 1000 pF.

Figure 9 shows the two-dimensional ion density profiles for different termination capacitances at 50 mTorr in H-mode. Black circles indicate the maxima of the azimuthal ion density distributions along the coil. The maximum point of the azimuthal ion density distribution rotates clockwise with an increase in the termination capacitance. The

position of the maximum point coincides with the virtual ground position (see Fig. 4), and they move together.

As we expected, there are minima and maxima in the azimuthal ion density distributions in E and H modes, respectively, and the positions of the minimum and maximum ion density move clockwise with increasing termination capacitance. The positions of the virtual ground agree well with Fig. 4. The density variation is up to 7% in H-mode and up to 50% in E-mode. As a result, the electron and ion density profiles can be controlled by adjusting termination capacitor at higher pressure.

IV. CONCLUSION

In this paper, changes of the electron and ion density profiles with the termination capacitance were observed in argon inductively coupled plasma. At 2 mTorr, where the electrons are governed by non-local electron kinetics, the electrons can travel the entire volume of the plasma before losing their energy, and the ionization reaction takes place in the entire volume of the plasma. As a result, the electron and ion profiles are determined by ambipolar diffusion, and the overall densities change with the termination capacitance but there are little changes to the electron and ion profiles with the termination capacitance. However, at 50 mTorr, the electrons are governed by local electron kinetics, and the electron and ion density profiles are remarkably changed with termination capacitance. In this regime, the electron and ion density profiles are determined by local heating and local ionization. Therefore, local capacitive coupling, which changes with the location of the virtual ground, changes the local heating and local energy loss, resulting in a significant change in the electron and ion density profiles. Our experimental results directly show the relationship between the capacitive coupling and the profiles of electron and ion density. Until recently, there has been little density control in the azimuthal direction, and this paper proposes a new method to control

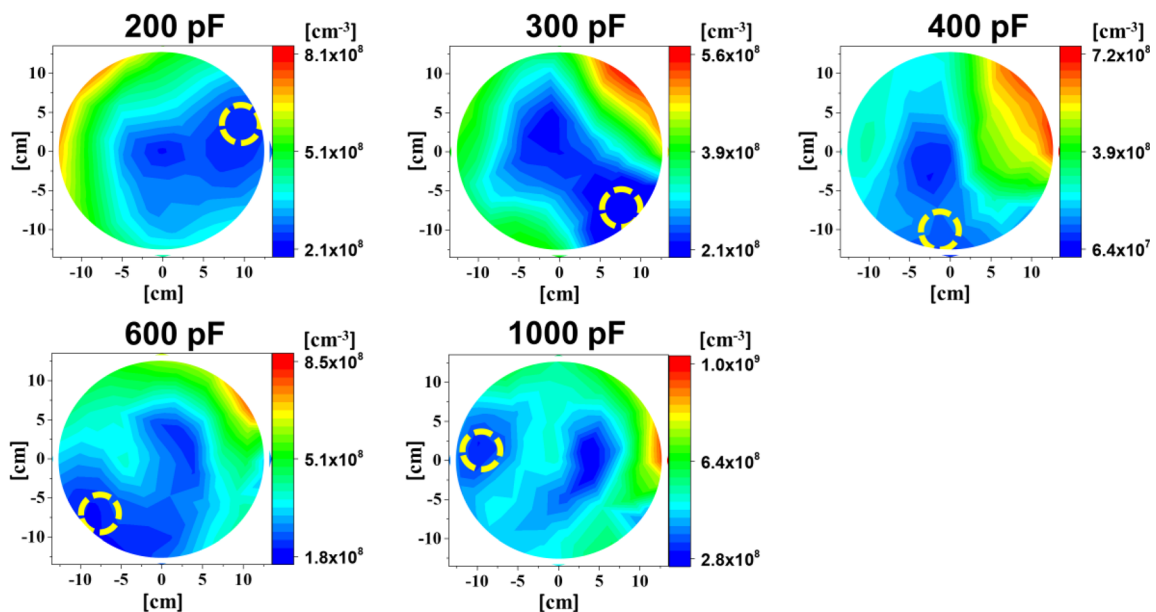


FIG. 8. Two-dimensional ion density profiles at 50 mTorr in E-mode with various termination capacitances.

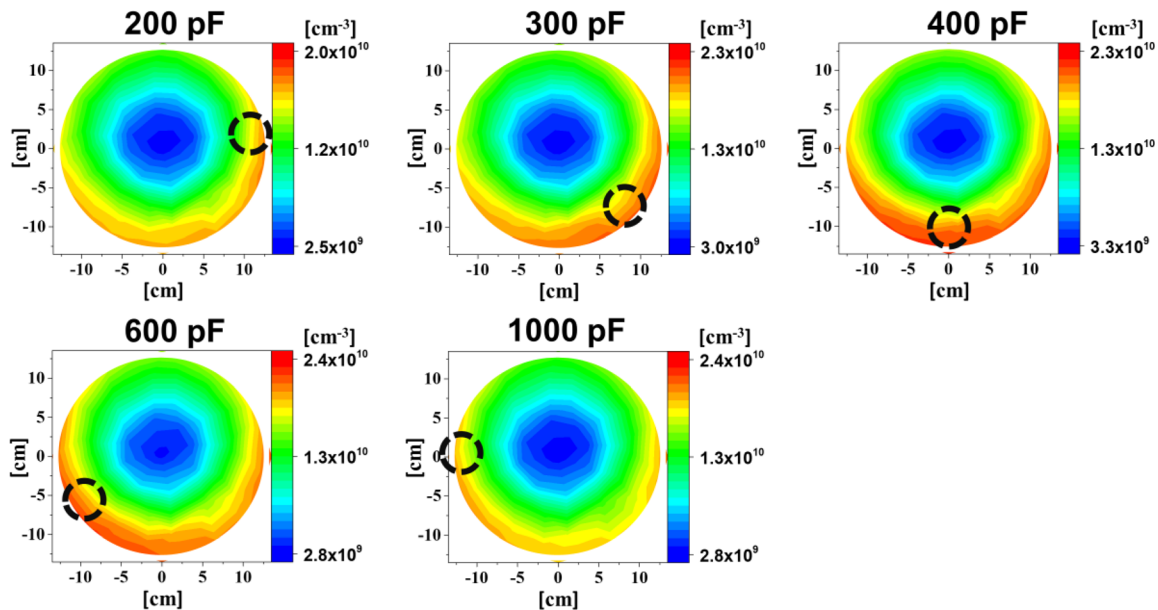


FIG. 9. Two-dimensional ion density profiles at 50 mTorr in H-mode with various termination capacitances.

density profile in the azimuthal direction. In addition, it is possible to control the radial direction by changing the structure of the coil. In our experiments, the electron and ion density changes occur in the azimuthal direction because the coil is a one-turn loop. However, this effect can also lead to electron and ion density changes in other directions by changing the structure of the coil. For example, if the coil is a double-spiral or multi-spiral coil, the virtual ground will move from the center of the chamber to the edge as the termination capacitance increases. Therefore, such a coil is able to control the electron and ion density profiles in the radial direction. Accordingly, this effect can be applied in many ways and is useful for generating a uniform plasma.

ACKNOWLEDGMENTS

This work was supported by the National Research Foundation of Korea (No. NRF-2019M1A7A1A03087579) and the Ministry of Trade, Industry and Energy (Nos. 10052861 and 20007145).

DATA AVAILABILITY

The data that support the findings of this study are available from the corresponding author upon reasonable request.

REFERENCES

- ¹N. S. J. Braithwaite, *Plasma Sources Sci. Technol.* **9**, 517 (2000).
- ²P. Chabert and N. Braithwaite, *Physics of Radio-Frequency Plasmas* (Cambridge University Press, 2011).
- ³M. A. Lieberman and A. J. Lichtenberg, *Principles of Plasma Discharges and Materials Processing* (John Wiley & Sons, 2005).
- ⁴T. E. Benson, L. I. Kamlet, S. M. Ruegsegger, C. K. Hanish, P. D. Hanish, B. A. Rashap, P. Klimecky, J. S. Freudenberg, J. W. Grizzle, and P. P. Khargonekar, *J. Vac. Sci. Technol., B* **14**, 483–488 (1996).
- ⁵F. M. Salam, C. Piwek, G. Erten, T. Grotjohn, and J. Asmussen, *IEEE Trans. Control Syst. Technol.* **5**, 598–613 (1997).
- ⁶J. Hopwood, *Plasma Sources Sci. Technol.* **1**, 109–116 (1992).
- ⁷J. H. Keller, J. C. Forster, and M. S. Barnes, *J. Vac. Sci. Technol., A* **11**, 2487–2491 (1993).
- ⁸J. H. Keller, *Plasma Sources Sci. Technol.* **5**, 166 (1996).
- ⁹H.-C. Lee, *Appl. Phys. Rev.* **5**, 011108 (2018).
- ¹⁰M. A. Sobolewski and J.-H. Kim, *J. Appl. Phys.* **102**, 113302 (2007).
- ¹¹H.-C. Lee, M.-H. Lee, and C.-W. Chung, *Appl. Phys. Lett.* **96**, 071501 (2010).
- ¹²F. Jan, A. Khan, A. Saeed, and M. Zakaullah, *Eur. Phys. J. D* **66**, 103 (2012).
- ¹³H.-C. Lee and C.-W. Chung, *Phys. Plasmas* **22**, 053505 (2015).
- ¹⁴M.-H. Lee and C.-W. Chung, *Phys. Plasmas* **13**, 063510 (2006).
- ¹⁵H.-C. Lee and C.-W. Chung, *Thin Solid Films* **521**, 185–188 (2012).
- ¹⁶F. Gao, S.-X. Zhao, X.-S. Li, and Y.-N. Wang, *Phys. Plasmas* **17**, 103507 (2010).
- ¹⁷M.-H. Lee, K. H. Lee, D.-S. Hyun, and C.-W. Chung, *Appl. Phys. Lett.* **90**, 191502 (2007).
- ¹⁸M.-H. Lee and C.-W. Chung, *Plasma Sources Sci. Technol.* **19**, 015011 (2010).
- ¹⁹H.-C. Lee, D.-H. Kim, and C.-W. Chung, *Appl. Phys. Lett.* **102**, 234104 (2013).
- ²⁰H.-C. Lee and C.-W. Chung, *Sci. Rep.* **5**, 15254 (2015).
- ²¹V. A. Godyak, R. B. Piejak, and B. M. Alexandrovich, *J. Appl. Phys.* **85**, 703–712 (1999).
- ²²H. Sugai, K. Nakamura, and K. Suzuki, *Jpn. J. Appl. Phys., Part 1* **33**, 2189 (1994).
- ²³K. Suzuki, K. Nakamura, H. Ohkubo, and H. Sugai, *Plasma Sources Sci. Technol.* **7**, 13–20 (1998).
- ²⁴W. Chen, K. Sugita, Y. Morikawa, S. Yasunami, T. Hayashi, and T. Uchida, *J. Vac. Sci. Technol., A* **19**, 2936–2940 (2001).
- ²⁵K. Nakamura, Y. Kuwashita, and H. Sugai, *Jpn. J. Appl. Phys., Part 2* **34**, L1686 (1995).
- ²⁶K. Suzuki, K. Konishi, K. Nakamura, and H. Sugai, *Plasma Sources Sci. Technol.* **9**, 199–204 (2000).
- ²⁷V. A. Godyak and B. M. Alexandrovich, *Rev. Sci. Instrum.* **88**, 083512 (2017).
- ²⁸K. Yoshida, H. Miyamoto, E. Ikawa, and Y. Mura, *Jpn. J. Appl. Phys., Part 1* **34**, 2089 (1995).
- ²⁹J.-H. Kim, H.-J. Lee, Y.-T. Kim, K.-W. Whang, and J.-H. Joo, *J. Vac. Sci. Technol., A* **15**, 564–567 (1997).
- ³⁰B. Zheng, M. Shrestha, K. Wang, T. Schuelke, E. Shun'ko, V. Belkin, and Q. H. Fan, *J. Appl. Phys.* **126**, 123302 (2019).
- ³¹M. Edamura and E. C. Benck, *J. Vac. Sci. Technol., A* **22**, 293–301 (2004).
- ³²F. Laerme, A. Schilp, K. Funk, and M. Offenberger, paper presented at the Technical Digest, IEEE International MEMS 99 Conference, Twelfth IEEE

- International Conference on Micro Electro Mechanical Systems (Cat. No. 99CH36291), 1999.
- ³³J. Hopwood, D. Reinhard, and J. Asmussen, *J. Vac. Sci. Technol., A* **8**, 3103–3112 (1990).
- ³⁴M. Ikegawa, J. I. Kobayashi, and R. Fukuyama, *J. Vac. Sci. Technol., A* **19**, 460–466 (2001).
- ³⁵R. Piejak, V. Godyak, and B. Alexandrovich, *Plasma Sources Sci. Technol.* **1**, 179 (1992).
- ³⁶M. Lieberman and R. Boswell, *J. Phys. IV* **08**, Pr7-145–Pr147-164 (1998).
- ³⁷I. D. Sudit and F. F. Chen, *Plasma Sources Sci. Technol.* **3**, 162 (1994).
- ³⁸Y.-C. Kim, S.-H. Jang, S.-J. Oh, H.-C. Lee, and C.-W. Chung, *Rev. Sci. Instrum.* **84**, 053505 (2013).
- ³⁹M.-H. Lee, S.-H. Jang, and C.-W. Chung, *J. Appl. Phys.* **101**, 033305 (2007).
- ⁴⁰I.-S. Park, H.-J. Kang, K.-H. Kim, and C.-W. Chung, *Phys. Plasmas* **24**, 123506 (2017).
- ⁴¹D. Nikandrov and L. Tsendin, *Tech. Phys. Lett.* **32**, 719–724 (2006).
- ⁴²L. D. Tsendin, *Phys.-Usp.* **53**, 133 (2010).
- ⁴³L. Tsendin, *Plasma Sources Sci. Technol.* **18**, 014020 (2009).
- ⁴⁴U. Kortshagen and L. D. Tsendin, *Electron Kinetics and Applications of Glow Discharges* (Springer Science & Business Media, 1998).
- ⁴⁵L. D. Tsendin, *IEEE Trans. Plasma Sci.* **34**, 728–737 (2006).
- ⁴⁶F. F. Chen, *Introduction to Plasma Physics and Controlled Fusion* (Springer, 1984).
- ⁴⁷S. F. Biagi, see www.lxcat.net for information about electron/argon impact cross section. (last accessed May 25, 2020).
- ⁴⁸V. A. Godyak and R. B. Piejak, *Phys. Rev. Lett.* **65**, 996–999 (1990).
- ⁴⁹C. Chung and H.-Y. Chang, *Appl. Phys. Lett.* **80**, 1725–1727 (2002).
- ⁵⁰V. A. Godyak, V. P. Meytlis, and H. R. Strauss, *IEEE Trans. Plasma Sci.* **23**, 728–734 (1995).
- ⁵¹M. H. Lee, H. C. Lee, and C. W. Chung, *Phys. Rev. E* **81**, 046402 (2010).
- ⁵²E. V. Karoulina and Y. A. Lebedev, *J. Phys. D* **21**, 411–417 (1988).